minerals

MDPI

Article

Copper-Bearing ("Paraíba") Tourmaline from Abuloo, Ethiopia: Preliminary Results

Stefanos Karampelas [1,*], Ugo Hennebois [2], Emmanuel Fritsch [3], Haimanot Sisay [4], Léonard Cornuz [1], Quentin Dartois [2], Aurélien Delaunay [2] and Vincent Pardieu [5]

[1] Department of Mineralogy-Petrology-Economic Geology, School of Geology, Aristotle University of Thessaloniki, 54124 Thessaloniki, Greece
[2] Laboratoire Français de Gemmologie (LFG), 30 rue de la Victoire, 75009 Paris, France
[3] IMN, Institut des Matériaux de Nantes Jean Rouxel, Centre National de la Recherche Scientifique, Nantes Université, 44000 Nantes, France
[4] Africa Gemological Training Institute (AGTI), Ras Mekonnen Avenue, Addis Ababa 1000, Ethiopia
[5] VP Consulting WLL, Manama, Bahrain
* Correspondence: skarampelas@geo.auth.gr

Abstract

A series of tourmalines from Abuloo, Oromia regional state, Ethiopia, was studied to describe their chemical and spectroscopic characteristics. Data from the seven samples were consistent with elbaite. Several specimens contained significant concentrations of copper (up to 2.29 wt%) and iron up to 0.81 wt%. Visible absorption spectroscopy indicated that the blue coloration in most samples is primarily related to Cu, with Mn and Fe contributing to a lesser extent, whereas in some specimens, Fe is the chromophore dominating Cu. The Cu-dominant tourmalines exhibited characteristics that correspond to the gemological definition of Paraíba tourmaline. Elements such as Ga, Pb, Bi, Zn, and V, as well as REE and Cu, could help to distinguish Ethiopian samples from copper-bearing tourmalines from Brazil, Mozambique, and Nigeria. These results suggest that the Abuloo occurrence represents a potentially significant source of gem-quality, unheated Cu-bearing tourmaline with distinctive features that may aid in its identification.

Keywords: tourmaline; copper-bearing; Paraíba; Ethiopia; Abuloo

1. Introduction

Gem-quality tourmaline, blue to green in color due to copper, was first discovered in the state of Paraíba in northeastern Brazil in the late 1980s [1–7]. These gems became known as Paraíba tourmalines after the locality of their discovery. Over the past thirty years, tourmalines of a similar color have also been discovered in several other mining areas in Rio Grande do Norte State, Brazil, Oyo State, Nigeria, and Nampula Province, Mozambique [8–25]. Today, gemmological laboratories consider Paraíba tourmaline to be a blue tourmaline ("electric" blue, "neon" blue, violet blue), bluish-green, green, or yellowish-green, with medium-light to high saturation and hue, mainly due to the presence of copper and manganese, regardless of geographical origin [26]. For this reason, the term Paraíba tourmaline will be used throughout the text, rather than the term Paraíba-type tourmaline, which is sometimes used.

Paraíba tourmalines are lithium-rich and generally consist of elbaite (fluor-elbaite, referred to simply as elbaite throughout this text) and rarely of liddicoatite (fluor-liddicoatite, here simply referred to as liddicoatite); only some Paraíba tourmalines from Mozambique

Check for updates

Academic Editors: Guanghai Shi and Tianlong Jiang

Received: 7 September 2026
Revised: 17 September 2026
Accepted: 19 September 2026
Published: 21 September 2026

Copyright: © 2026 by the authors. Licensee MDPI, Basel, Switzerland. This article is an open access article distributed under the terms and conditions of the Creative Commons Attribution (CC BY) license.

have been included in the latter group [21,22,24,27,28]. To date, no Paraíba tourmalines belonging to the rossmanite species are known [29,30]. Most gem-quality Paraíba tourmalines available on the market have been heat-treated [5,16,20,24,25,31].

Gem-quality tourmalines exhibit a wide range of colors, resulting from the presence of various transition elements, such as Ti^{4+}, V^{3+}, Cr^{3+}, Mn^{2+}, Mn^{3+}, Fe^{2+}, Fe^{3+}, and Cu^{2+}, as well as radiation-induced color centers that act as chromophores [30]. According to the generally accepted classification of Henry et al., 2011 [32], more than 40 species of tourmaline are currently recognized, and their correct identification requires accurate chemical analyses [22,29,32]. Among the gem-quality tourmalines, elbaite is the predominant species, although gems made of liddicoatite, rossmanite, dravite, and uvite are also found on the market, as well as some black tourmalines used in jewelry, which belong to the schorl or foitite species [29,30].

Paraíba tourmalines are arguably the most highly sought-after and most expensive varieties of gem-quality tourmaline [24,30], hence the interest in the new Ethiopian deposit. However, tourmalines with similarly intense and pure blue coloration are colored by iron rather than copper [27,30,31,33]. In the gem trade, such tourmalines are sometimes referred to as indicolites or "lagoon" tourmalines and occur in Namibia and Afghanistan, as well as other countries [33,34]. Their coloration is due to the rather unique Fe^{2+}–Fe^{3+} exchange interaction in the "Y trimer", which is unique to the tourmaline structure: this phenomenon intensifies Fe^{2+} absorptions (without modifying their position) and generates a very strong pleochroism. Cuprian tourmalines have a comparatively moderate pleochroism [35].

The presence of copper does not necessarily mean that the tourmaline has copper as a chromophore. In some cases, copper may be present within inclusions in tourmalines that exhibit Fe-based coloration similar to that of true Paraíba tourmalines [27,36–38]. Optical absorption spectroscopy demonstrates that iron is the main chromophore and, consequently, such stones should not be classified as Paraíba tourmalines [27].

Paraíba tourmalines are associated with pegmatitic environments; however, the source of copper remains uncertain across all known mining areas. In Brazil, most of these gems are mined from primary deposits, whereas in Nigeria and Mozambique, they are mainly found in secondary deposits [27]. The geographic origin of Paraíba tourmalines is significant, as in general tourmalines from Brazil are more highly sought after in the gem trade than those from other countries. Paraíba tourmalines of different origins cannot be clearly distinguished under the microscope, but their trace-element and isotope composition differs from one country to another [16,23–25,39–41]. Identification is based not on the specific mining area, but rather on the geographic origin, using non-destructive (or, in rare cases, micro-destructive) methods that are cost-effective in terms of both equipment requirements and analytical time [42–45]. Today, a combination of trace-element chemical analysis, microscopy, and absorption spectroscopy is currently used to determine the origin of Paraíba tourmalines, a process that is successful in most cases [16,24,25].

In May 2026, several samples reportedly identified as Paraíba tourmalines from Ethiopia appeared on the market and were examined by one of the authors (HS). HS, in collaboration with other authors (VP and LC), collected important information about this material, and subsequently HS visited the mining area. At the same time, newsletters and social media by different gem labs and gemologists initially suggested that Ethiopian samples could potentially be misidentified as Brazilian material and, some days later, that they display a distinctive trace-element profile [46–52]. Some contributions also highlighted that not all of the samples examined can be classified as Paraíba tourmalines [47,48]. The authors of the present study contributed to social media posts presenting preliminary results obtained from some samples from the area as well as to a field report documenting their visit to the mining area [47,49,50]. Several rough samples of gem quality can weigh

well above 40 carats [49]. In this study, we present a characterization of samples from Abuloo, Ethiopia, based on microscopic, spectroscopic, and chemical data, integrated with a presentation of their geological context. This work aims to demonstrate that some of these Ethiopian tourmalines can be classified as *bona fide* Paraíba tourmalines.

2. Materials and Methods

Seven unheated rough tourmalines from Abuloo, Oromia regional state (Ethiopia), were studied (Figure 1 and Table 1). Samples collected in the field, directly by the scientist, were characterized as A-type and had the highest degree of reliability, while stones characterized as F-type came from international markets [53]. The studied samples were donated to VP in Bangkok in early June 2026 by a gem dealer who had purchased a significant lot in Ethiopia a few days earlier. Thus, the cataloguing classification falls under the F type. All samples were slightly polished to facilitate the analyses. All data presented in Figure 1 and Table 1 were obtained after polishing.



Figure 1. The seven tourmalines are light to dark blue in color and range from 0.13 ct for the smallest sample, ETH#15, measuring 3.90 × 2.09 × 1.66 mm, to 2.77 ct for the largest sample, ETH#17, measuring 9.02 × 7.77 × 4.45 mm.

Table 1. Dimensions and weight of the seven blue tourmalines from Ethiopia investigated in this study (1 carat -ct- = 0.2 g).

Sample Number	Dimensions (mm)	Weight (ct)
ETH#15	3.90 × 2.09 × 1.66	0.13
ETH#16	9.28 × 3.40 × 2.52	0.75
ETH#17	9.02 × 7.77 × 4.45	2.77
ETH#18	8.12 × 4.68 × 3.30	1.19
ETH#19	4.71 × 3.79 × 2.27	0.48
ETH#20	5.21 × 4.05 × 3.78	0.74
ETH#21	7.49 × 6.88 × 3.17	1.57

For the optical observation of all samples and their inclusions, a Zeiss Stemi 508 binocular microscope (Carl Zeiss Microscopy Deutschland GmbH, Oberkochen, Deutschland) was used (FOV, field of view, represents the width of the photo measured in mm). An ultraviolet (UV) luminescence reaction was observed for all samples under a 6 W lamp (Vilber Lourmat VL-6.LC; Vilber Lourmat Deutschland GmbH, Eberhardzell, Germany) with 365 nm (long-wave ultraviolet—LWUV) and 254 nm (short-wave ultraviolet -SWUV) excitation, equipped with a CN-6 dark room (10 cm distance between samples and the lamp). The Raman and photoluminescence (PL) spectra were acquired with a micro-Raman

Renishaw inVia spectrometer (Renishaw plc, Wotton-under-Edge, Gloucestershire, UK), coupled with an optical microscope and a 514 nm laser excitation (diode-pumped solid-state laser). Raman spectra in the 200 to 1500 cm^{-1} and 3200 to 3800 cm^{-1} ranges were obtained with 2 accumulations and a 10 s exposure time with laser power at 100%. PL spectra (800–950 nm) were acquired with 10 s of exposure time, 1 accumulation, and 10% laser power. The Raman spectrometer was calibrated with a diamond, considering its Raman peak to be at 1331.8 cm^{-1}. For visible-near infrared (Vis-NIR) spectroscopy (from 365 to 1000 nm), a mobile GemmoSphere instrument by Magilabs (Järvenpää, Finland) was used, equipped with an integrating sphere, and with an acquisition time of 0.05–0.50 s and 20 accumulations.

A laser ablation-inductively coupled plasma-mass spectrometry (LA-ICP-MS) chemical analysis was performed at the Laboratory of Planetology and Geosciences (LPG UMR 6112), Nantes University, France, using an Agilent 8900 Triple Quadrupole (Agilent Technologies Inc.; Santa Clara, CA, USA) inductively coupled plasma-mass spectrometer (ICP-MS) coupled with a femtosecond laser IRIDIA femto operating at a wavelength of 257 nm (Teledyne Photon Machines, Bozeman, MT, USA). A laser spot of 60 µm in diameter was used, together with a fluence of around 3 J/cm^2 and a 10 Hz repetition rate. Three spots were analysed in every sample. For the ICP–MS operations, the forward power was set at ~1510 W, and the dwell time for each isotope was fixed at 15 ms. The acquisition signal was composed of 3 different parts: 30 s for blank, 30 s for signal, and 30 s for washout. The criteria for the alignment and tuning sequence were established on NIST610 glass. The criteria were used to maximize the intensity counts for all elements, keep the U/Th ratio at around 1, and maintain the ThO/Th ratio below 0.4%. NIST 610 and NIST 612 glasses as calibration standards. The time-resolved signal was processed with GLITTER version 4.4.4 software using silicon SiO_2 as the internal standard, applying the 39.33 wt% theoretical value for tourmalines. Several isotopes were measured for all samples; however, only a selected few are presented here, those which matter [24] to determine the tourmaline species, geographic origin determination, and measure the concentration of chromophores. The selected isotopes are as follows: ^{23}Na, ^{44}Ca, ^{51}V, ^{52}Cr, ^{55}Mn, ^{57}Fe, ^{63}Cu, ^{66}Zn, ^{71}Ga, ^{85}Rb, ^{88}Sr, ^{118}Sn, ^{208}Pb, and ^{209}Bi.

3. Results and Discussion

3.1. Geology

Tourmalines were found in secondary deposits in Abuloo, Oromia regional state/region, southern Ethiopia (Figure 2) [24]. The Precambrian basement of southern Ethiopia is part of the East African Orogen, which developed during the Neoproterozoic assembly of Gondwana. Southern Ethiopia lies within the tectonic transition between the Arabian-Nubian Shield and the Mozambique Belt and comprises medium- to high-grade metamorphic and plutonic rocks [54,55]. Within this basement, the Adola Belt constitutes a complex domain divided into granite-gneiss complexes (GGC), including the Adola and Genale-Dolo complexes, and ophiolitic fold-and-thrust belts (OFTB), including the Megado, Kenticha, and Bulbul mafic–ultramafic and volcano-sedimentary belts [54]. The whole Adola Belt was subsequently intruded by late- to post-orogenic granites, some of them highly fractionated (see again, Figure 2) [56]. The Adola Belt hosts several mineral systems, such as the orogenic gold at Lega Dembi Mine [57,58], the Ta-Li-Be pegmatite at the Kenticha Mine [56], and the tectonic-magmatic-related emerald occurrence known as the Halo-Shakiso emerald field [59].

The gem rush was reported on the eastern side of the village of Abuloo (also spelt Abulo Rukesa [60]) in an area with very rare outcrops, often covered by reddish-brown sandy soil and visible only in some sections of the riverbed [61]. It was previously presented

as a soft soil hosting tourmaline crystal from the surface down to a depth of 6 m [49,50]. Based on this location and on the satellite signature of the gem rush, the area stands in a metasediment group of the Precambrian basement. This group was described in [61,62], without categorizing it in a specific P-T domain, as a high-grade metamorphic, intercalated quartzofeldspathic schist and gneiss correlated to the Zembaba Formation [63], possibly the lowermost tectonic unit of the Adola Belt [64] (Figure 3). The group was also interpreted as the Lower Wadera Metasediments, composed of quartzo-feldspathic schists, in places gneissic and migmatized, intercalated with quartzite beds [65]. In the continuous zone south of the area, the same unit has been described more as a quartzofeldspathic mylonite, with minor presence of quartzofeldspathic gneiss, biotite-plagioclase-microcline-quartz gneiss, and biotite granite [60]. Structurally, this unit is strongly sheared on the east and locally ultramylonitic, with NW-SE mylonitic foliations interpreted as synthetic shear fractures associated with the Wadera Shear Zone [60]. For other lithologies present in the area, the post-tectonic granitoid intrusions form several summits north of the area (Mt. Galo, Mt. Walal). Those intrusions are strongly weathered and exfoliated, forming a sharp contact with the surrounding lithologies. The foliation deflected around these granitic intrusions, indicating that the country rocks were still ductile during granite emplacement [60].

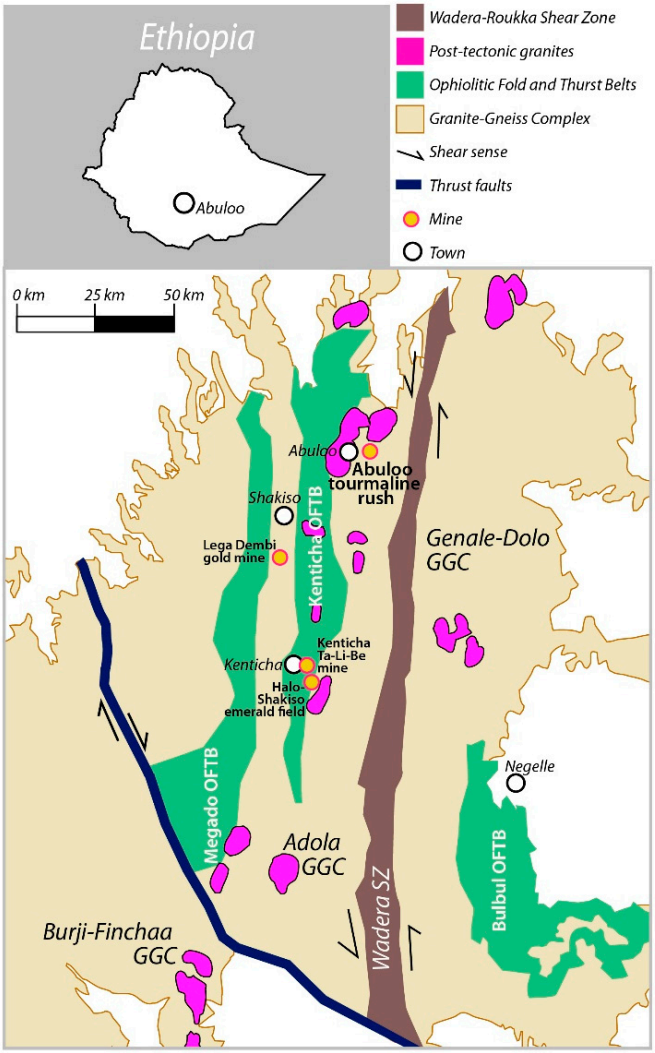


Figure 2. Tectonic map of the Adola Belt simplified after [54,65].

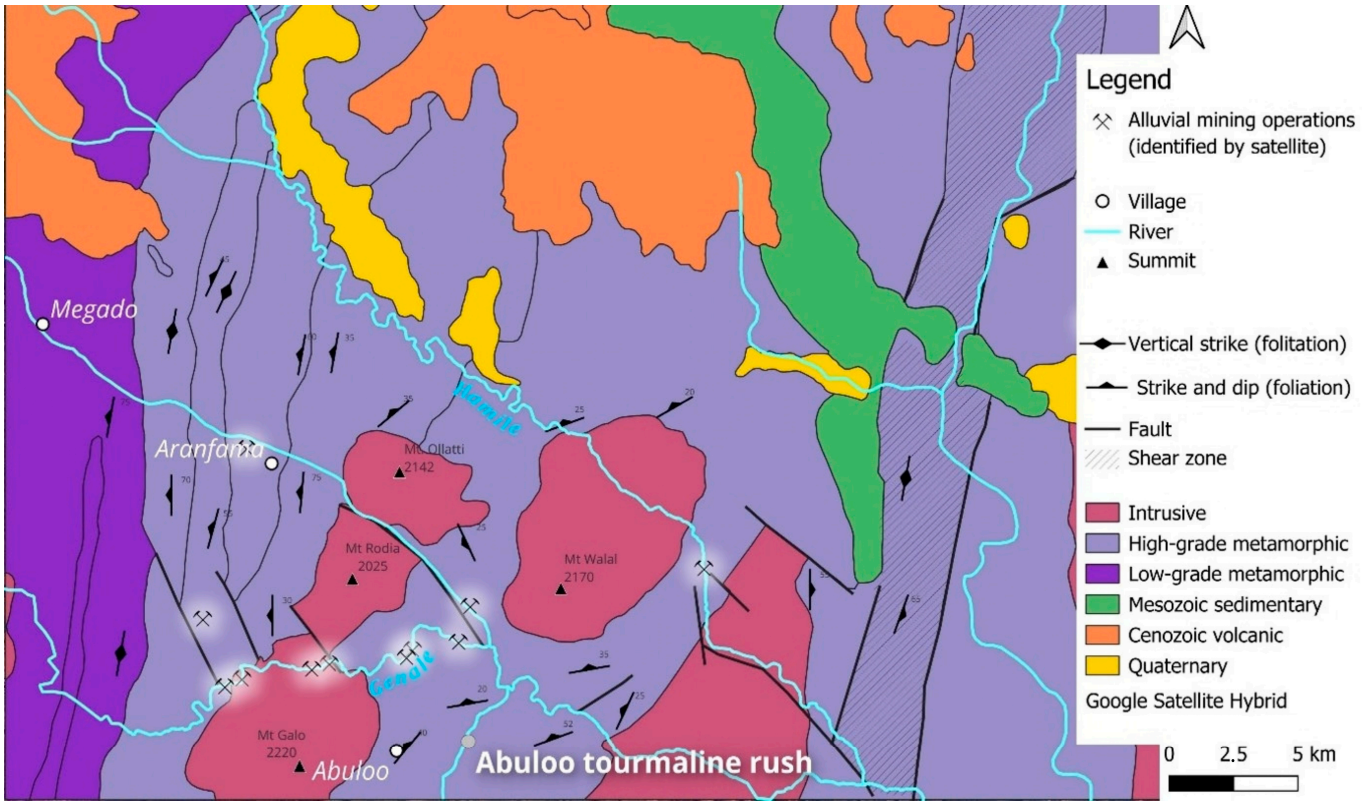


Figure 3. Geology of the area of interest; the different units are classified according to their rock type, modified after [61]. Note the focus of the alluvial gold mining operations along the Genale River for the period 2025–2026.

Pb–Pb zircon ages from gneissic rocks in the Zembaba–Wadera corridor, approximately 7–25 km south to southeast of the village of Abuloo, indicate that these units are not contemporary [66]. A porphyritic granite gneiss at Zembaba crystallized at 752.3 ± 0.6 Ma, whereas the mylonitic Alghe augen gneiss preserves a tonalitic protolith age of 559.9 ± 0.9 Ma; both ages predate the subsequent deformation and mylonitization of the rocks.

Locally, in the town of Abuloo, pegmatites are noted to intrude the unit and form veins up to 5 cm wide, with magnetite in the quartz veins and veinlets [60]. Geochemical surveys in the Kenticha–Katawicha area recorded isolated Cu enrichments exceeding 63 ppm, mainly east and west of the meta-ultramafic bodies. The Ethiopian Institute of Geological Survey [67] attributed these anomalies to amphibolite intercalations in biotite gneiss and, locally, to amphibolite rafts within the heterogeneous Gariboro granite-gneiss. Although the Adola district is well known for its major mineral deposits, the geological setting of the Abulo gem occurrence remains poorly understood. Field mapping is essential to identify the unit and the source of the gem-bearing material at Abuloo.

3.2. Classical Gemology

The seven studied samples are transparent with a light to dark blue color (Figure 1). Their mass ranges from 0.13 to 2.77 ct; their dimensions and weights are listed in Table 1. All samples are inert under SWUV and LWUV lamp excitation. All samples present pleochroism; the strongest pleochroism observed is for ETH19, with the other samples presenting weak to medium pleochroism (Figure 4a–d). All samples contain inclusions visible under the optical microscope, including growth tubes, multiphase inclusions, and fissures containing yellow-colored epigenetic material (Figure 5a–d).

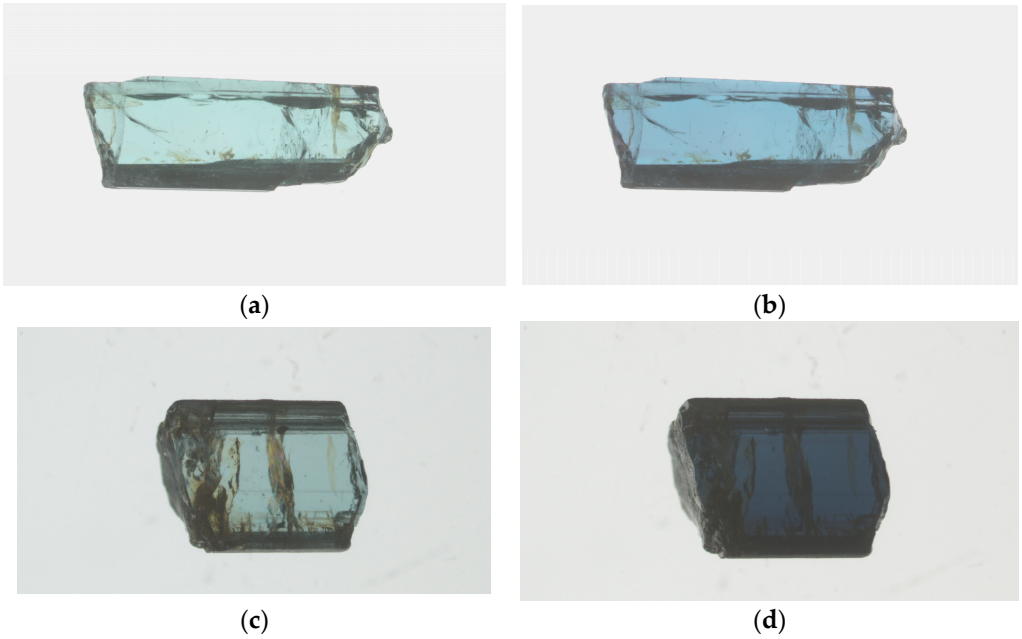


Figure 4. Sample ETH#16 (9.28 × 3.40 × 2.52 mm) under microscope without polarizer (**a**) and with polarizer (**b**), as well as ETH#19 (4.71 × 3.79 × 2.27 mm) without polarizer (**c**) and with polarizer (**d**). Sample ETH#16 presents medium pleochroism, and sample ETH#19 presents strong pleochroism. Photos by Ugo Hennebois; LFG.

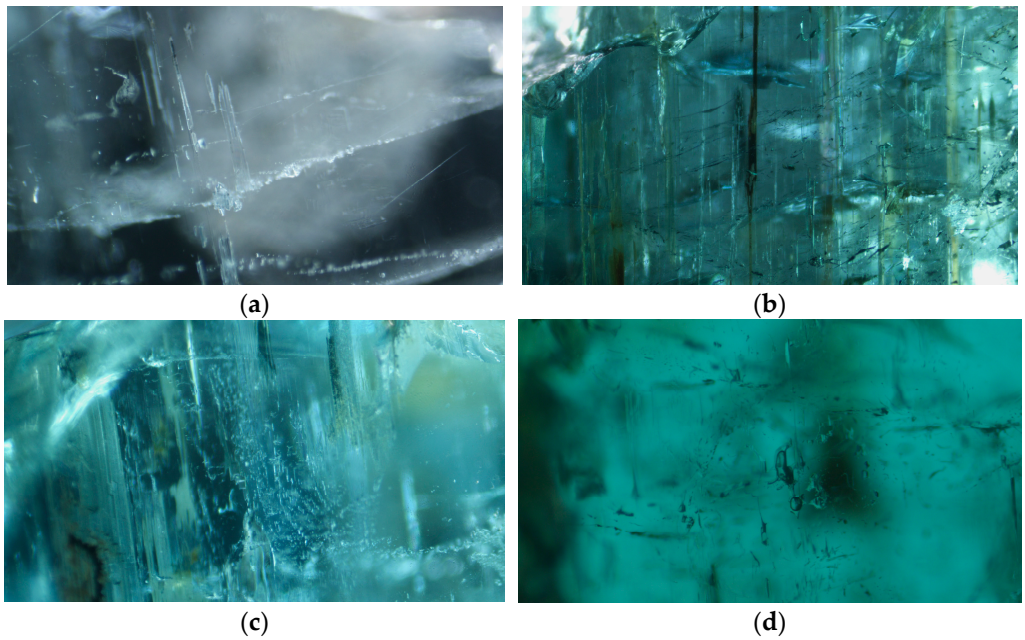


Figure 5. Microscopic features of the studied tourmalines from Ethiopia. (**a**) Fluid inclusions and growth tubes (ETH#15); FOV: 1 mm, (**b**) growth tubes, fissures, and yellow epigenetic material (ETH#17); FOV: 2 mm, (**c**) multiphase inclusions and growth tubes (ETH#20); FOV: 1.5 mm, (**d**) multiphase inclusions (ETH#21); FOV: 0.8 mm. Photos by Ugo Hennebois; LFG.

3.3. Spectroscopy

Raman spectra were collected from all the samples; Figure 6 illustrates the Raman spectra of three representative samples from 200 to 1200 cm^{-1} (fundamental vibrations region) and from 3200 to 3800 cm^{-1} (OH stretching region). All samples produced similar spectra, with bands situated at 374, 712 and 1092 cm^{-1}, all linked to tourmaline vibrations, with small differences in relative band intensities which may be attributed to crystallographic

orientation effects. The hydroxyl (OH) stretching region is useful to separate tourmaline species, in particular liddicoatite and elbaite, even in randomly oriented crystals. Liddicoatite presents the main OH band slightly above 3600 cm^{-1}, and for elbaite it is slightly below 3600 cm^{-1} [27,68]. All spectra presented their main Raman OH band at around 3590 cm^{-1} (Figure 6b) and were thus consistent with elbaite tourmalines.

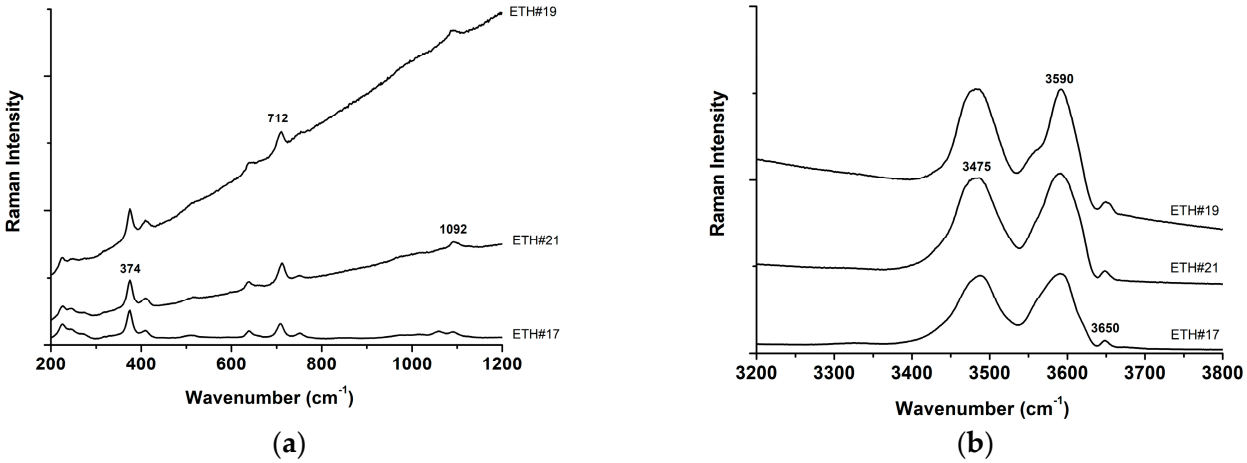


Figure 6. Raman spectra of three representative tourmalines in both the fundamental vibrations fingerprint (**a**) and OH stretching (**b**) regions. All samples present similar spectra, and in the OH region the main band is around 3590 cm^{-1}, consistent with elbaite. Spectra shifted vertically for clarity.

Vis-NIR absorption spectroscopy is an important tool for identifying Paraíba tourmalines, as Cu^{2+} presents two strong absorption bands at around 700 and 920 nm, with the second one more intense [5,7,24,31,69–71]. An absorption band at around 720 nm can be observed in tourmalines due to Fe^{2+}, sometimes enhanced by Fe^{2+}–Fe^{3+} exchange interactions (see above). A relatively broad band at around 520 nm and a couple of sharp bands at around 415 nm arise from Mn^{3+} and Mn^{2+}, respectively [5,17,20,31]. These bands are also dependent on crystallographic orientation [5,7]. However, in the present study, the spectra were acquired in a random orientation. Figure 7 presents the Vis-NIR absorption spectra of three samples. Two crystals (ETH#15 and ETH#16) have the strongest absorption at around 920 nm, with a less intense one at 700 nm. This corresponds to a nearly pure Cu^{2+} signal; thus, these gems may be classified as Paraíba tourmalines. In one sample (ETH#19), a strong Fe^{2+} absorption band is observed at around 720 nm. Thus, the copper-related bands contribute to a lesser extent, and the tourmaline is not considered "Paraíba". It is noteworthy that this is the only sample exhibiting strong pleochroism. Cu^{2+} induces local distortion upon entering the natural elbaite structure, in contrast to the behavior observed in some synthetic tourmalines [70,71].

In Figure 8, the spectra of samples ETH#17 and ETH#21 are presented. There is total absorption (sometimes incorrectly called "saturation") in the 700–1000 nm region, leading to bands being flattened and the signal/noise ratio being reduced. More precisely, the signal exceeds the dynamic range of the instrument in this part of the electromagnetic spectrum [69], resulting in very little light reaching the detector in the red and near-infrared; thus, the true spectral shape is not obtained. The spectra of the other two samples (ETH#18 and ETH#20) presented similar phenomena. In our specific, practical case (random orientation and thickness not controlled), the relative values of the absorbance at 900 nm and 700 nm (A_{900}/A_{700}) cannot be an effective means to separate Paraíba from non-Paraíba tourmalines [27], as the individual contributions of iron and copper to the visible absorption spectra cannot be reliably interpreted. This leaves the Cu/(Cu + Fe) ratio as a potential criterion, since it is not influenced by shape or thickness. Note that in relation to optical ab-

sorption, the strongest pleochroism is found for an iron-colored blue tourmaline (ETH#19). Cu^{2+} does not induce a strong pleochroism, and Paraiba tourmalines have only moderate to weak blue pleochroism.

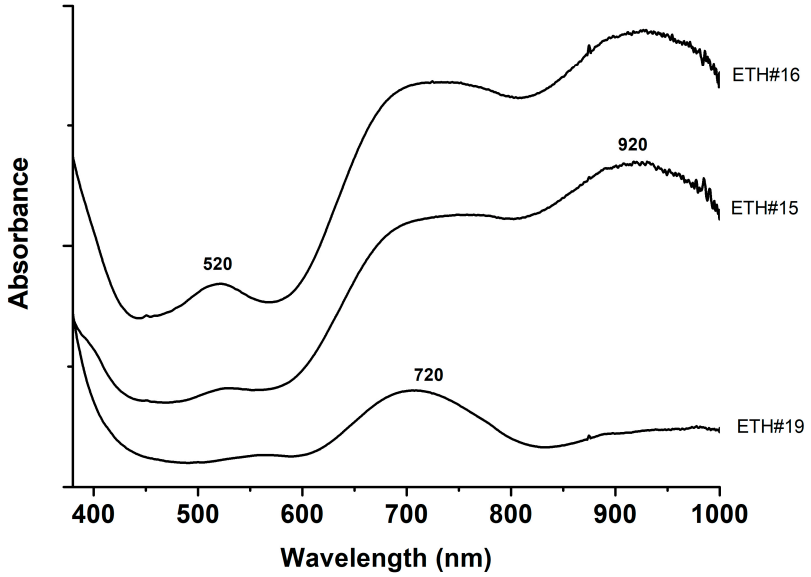


Figure 7. Vis-NIR absorption spectra of three samples. The bottom spectrum exhibits dominant absorption at around 720 nm related to Fe^{2+}, whereas the other two spectra present a band at 920 nm together with one at 700 nm due to Cu^{2+}. Thus, the top two can be classified as Paraíba tourmalines. An additional band at around 520 nm (more visible in the top spectrum) due to Mn^{3+} is also observed. Spectra shifted vertically for clarity.

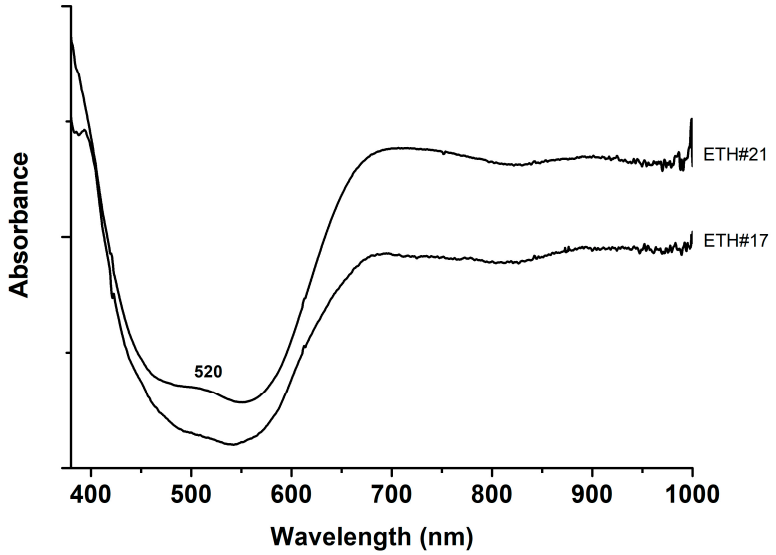


Figure 8. Vis-NIR absorption spectra of two samples for which total absorption is observed over 700 nm, deforming the true spectral shape. Spectra shifted vertically for clarity.

Photoluminescence (PL) spectroscopy has also been previously used to distinguish between elbaite and liddicoatite Paraiba tourmalines, based on a series of bands in the 850–950 nm region that are not polarization-dependent, with the main band situated at around 870 nm. They were stated to be encountered only in liddicoatite [72,73]. In Figure 9, the PL spectra of three samples are presented, where this characteristic series of bands is observed. These PL spectra bands are most likely associated with the presence of REE^{3+}, possibly Nd^{3+}, which may substitute for calcium [74]. Calcium occurs at higher

concentrations in liddicoatite tourmalines, although it is also present in elbaite tourmalines as an impurity (see Section 3.4 below). This confirms that this PL band system may be present, if weaker, in elbaite tourmaline [27] and is not characteristic of liddicoatite.

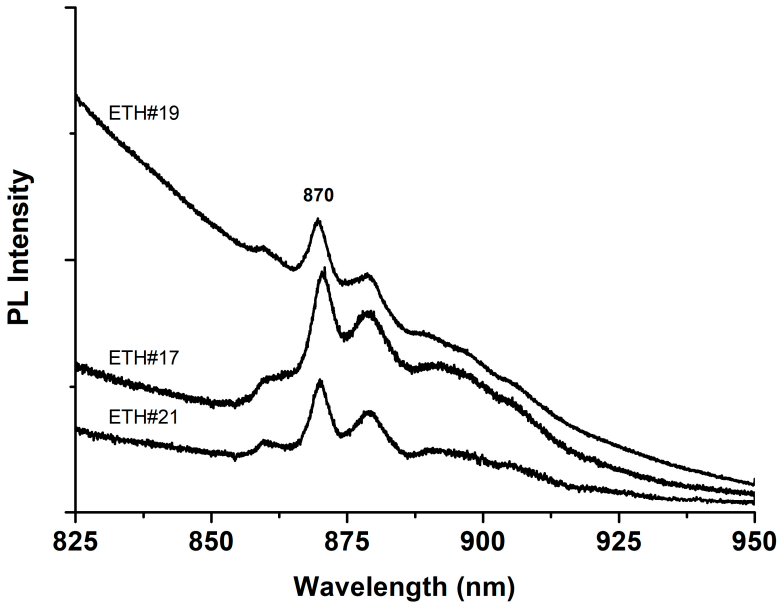


Figure 9. PL spectra of three samples obtained using 514 nm laser excitation. All samples present a series of bands, possibly related to Nd^{3+}, with the main band situated at around 870 nm. Spectra shifted vertically for clarity.

3.4. Chemistry

LA-ICP-MS analysis of the studied samples is presented in Table 2. Only selected elements relevant to tourmaline species determination, origin of color, and geographic origin determination are reported [24]. In all our tourmalines, the sodium concentration is higher than the calcium concentration, further confirming that the data for all samples are consistent with elbaite tourmalines. Furthermore, Cu/(Cu+Fe) is well above 0.6 in all but one (ETH#19), which is consistent with the criterion suggested for Paraíba tourmalines [27]. According to chemistry and visible absorption spectra, sample ETH#19 cannot be qualified as Paraíba tourmaline without ambiguity. Samples presenting total absorption in their randomly oriented visible absorption spectra contain elevated concentrations of copper up to 2.29% wt. In other words, if the color is due only to Fe-related absorption at about 720 nm, it is not possible to obtain total absorption at about 900 nm. Thus, all the other six samples can be called Paraíba tourmalines. In some of these tourmalines, the copper concentrations are so high that they are comparable only to those reported for Paraíba tourmalines from the historically significant mining area of São José da Batalha, Paraíba, Brazil [5,7].

The trace element chemistry of our Ethiopian Paraíba tourmalines differs from that reported for Paraíba tourmalines from Brazil, Mozambique, and Nigeria. In particular, gallium content is relatively high in the Ethiopian samples, exceeding 500 ppm (ppmw), a concentration measured only in a small number of Paraíba tourmalines from Mozambique [24]. Lead content can also be high in our gems. In Figure 10, we completed our data with binary plots that have been previously proposed to distinguish Paraíba tourmalines from different origins [24]. The Ethiopian samples occupy a distinct region in the examined binary diagrams and can be distinguished from those of other geographic origins (see again Figure 10). In addition, as previously reported in a newsletter, vanadium concentration is above 60 ppm in the Ethiopian samples, thus higher than the reported concentration

of Paraíba tourmalines from other countries [50]. Bismuth content is also high in some samples, and neodymium is present in all samples. Relatively high concentrations of Ga, Pb, and Bi can cause structural disorder in the tourmaline crystal structure; this needs further investigation in future studies [75–78].

Table 2. Data of chemical analysis on selected elements [24], as well as chromophores, ^{146}Nd, and ^{209}Bi. All values are in ppm except the values of ^{23}Na, ^{44}Ca, and ^{63}Cu (in grey matrix), which are in wt %. The data presented are the average values of the three analyses for each sample. LOQ for ^{88}Sr and ^{118}Sn is around 0.7 ppm. See the Supplementary Materials for the data from three individual points.

	ETH#15	ETH#16	ETH#17	ETH#18	ETH#19	ETH#20	ETH#21	Average [1]	Median [1]
^{23}Na	1.50	1.31	1.65	1.30	1.48	1.56	1.42	1.46	1.46
^{44}Ca	0.41	0.88	0.22	1.02	0.89	0.69	1.10	0.72	0.79
^{51}V	91.5	170	62.6	150	233	155	130	127	140
^{55}Mn	1421	3201	4861	3541	5784	4547	3676	3541	3609
^{57}Fe	173	222	6573	1104	8159	2757	2000	2138	1552
^{63}Cu	1.60	1.04	1.72	1.39	0.47	2.27	2.29	1.72	1.66
^{66}Zn	11.1	88.2	510	51.5	5465	150	115	154	102
^{71}Ga	822	888	747	690	369	719	568	739	733
^{88}Sr	<LOQ	5.65	1.67	5.29	75.7	4.31	6.86	3.96	5.29
^{118}Sn	8.34	12.7	13.0	6.58	<LOQ	7.77	10.9	9.88	9.62
^{146}Nd	11.0	13.9	2.10	17.5	9.27	14.4	59.2	19.7	14.2
^{208}Pb	457	1531	167	1277	2495	815	1167	902	991
^{209}Bi	166	1162	35.1	494	4615	330	423	435	377

[1] Average and median values are only for the Paraíba tourmalines; the analysis of sample ETH#19, which cannot be called a Paraíba tourmaline, is not included. These values are calculated without data for ETH#19.

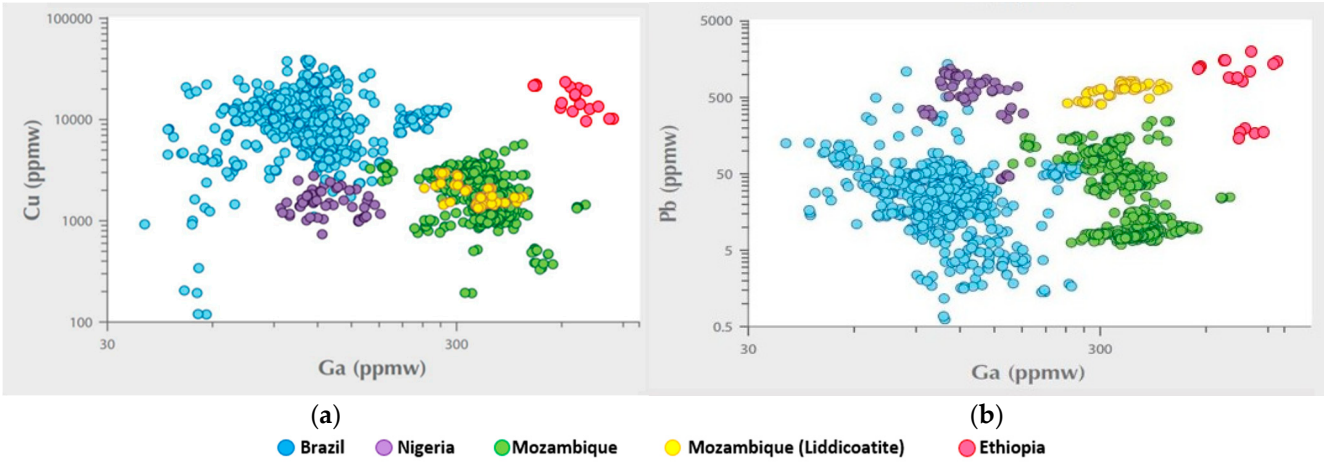


Figure 10. Binary plots of trace elements in Paraíba tourmalines from different mining areas [24] and our Ethiopian samples (**a**) Ga vs. Cu and (**b**) Ga vs. Pb. In both diagrams, the Ethiopian gems can be distinguished from those of other geographic origins.

4. Conclusions

A series of blue tourmalines from Ethiopia were studied in some detail to determine whether they may be called Paraíba tourmalines or not. Based on the current definition for Paraíba tourmalines, several Ethiopian samples clearly meet the requirements. The data on the studied Ethiopian Paraíba tourmalines are all consistent with elbaites and have trace element compositions distinct from those of Paraíba tourmalines from Brazil, Mozambique, and Nigeria, allowing them to be distinguished from samples from these

other geographic origins. Their distinctive chemical signatures can be measured using LA-ICP-MS or even EDXRF.

One of the studied samples cannot be classified as a Paraíba tourmaline because iron, rather than copper, is the main chromophore. This shows that not all tourmalines exhibiting a similar color from that mining area can be considered Paraíba tourmalines. The criteria previously proposed for identifying Paraíba tourmalines based on visible absorption spectroscopy and chemical composition [27] should also be applied with caution. In some cases, total absorption distorts the measured spectra (see Figure 8), making it difficult to reliably distinguish the individual contributions of iron and copper to the observed visible absorption features. However, the high copper and relatively low iron content in these tourmalines identify them as Paraíba tourmalines. All of the studied samples exhibit PL bands associated with REE^{3+} ions, possibly Nd^{3+}, which was also detected by LA-ICP-MS. Therefore, the use of these PL bands as a criterion for distinguishing between elbaite and liddicoatite should also be considered with caution.

All seven samples are unheated and display attractive colors. This represents an additional advantage for these stones, as unheated Paraíba tourmalines with good color are relatively rare in the market. However, several samples with purple or other colors can be found in the same area (Figure 11). These samples may potentially develop colors to be called Paraiba tourmalines after heat treatment, as their coloration is also related to Mn^{3+}, which may be reduced to Mn^{2+} during heating. Further study of additional samples from this mining area is necessary to confirm the differentiation criteria proposed here. A better understanding of the geology of the area is also essential for evaluating and revealing its full potential.



Figure 11. Tourmalines of various colors found in Abuloo, Ethiopia. Only some of the samples shown on the right were studied for the present report. The faceted stone in the front center weighs approximately 1 ct. Photo by Vincent Pardieu.

Supplementary Materials: The following supporting information can be downloaded at: https://www.mdpi.com/article/10.3390/min16090964/s1. The average values of the three analyses for each sample.

Author Contributions: Conceptualization, V.P. and S.K.; methodology, U.H. and S.K.; software, S.K.; validation, E.F., A.D., and S.K.; data curation, U.H., Q.D., E.F., H.S., and L.C.; writing—original draft preparation, S.K.; writing—review and editing, V.P., U.H., E.F., H.S., L.C., Q.D., and A.D.; supervision, S.K.; project administration, V.P. All authors have read and agreed to the published version of the manuscript.

Funding: This research received no external funding.

Data Availability Statement: Data are contained within the article.

Acknowledgments: The authors warmly thank Carole La, responsible for the LA–ICP–MS facility at the Laboratory of Planetology and Geosciences (LPG UMR 6112)—Nantes University, for her valuable input during the LA-ICP-MS analyses. During the preparation of this manuscript, the authors used ChatGPT 5 for the purposes of polishing the language. The authors have reviewed and edited the output and take full responsibility for the content of this publication.

Conflicts of Interest: Vincent Pardieu is an employee of VP Consulting WLL. The paper reflects the views of the scientists and not the company. The remaining authors declare no conflict of interest.

References

1. Koivula, J.I.; Kammerling, R.C. Unusual tourmalines from Brazil. *Gems Gemol.* **1989**, *25*, 181–182. [CrossRef]
2. Hargett, D.; Kane, R. Blue tourmaline from Brazil. *Gems Gemol.* **1989**, *25*, 241–242. [CrossRef]
3. Koivula, J.I.; Kammerling, R.C. Paraíba tourmaline update. *Gems Gemol.* **1989**, *25*, 248–249. [CrossRef]
4. Bank, H.; Henn, U.; Bank, F.H.; von Platen, H.; Hofmeister, W. Leuchtendblaue Cu-führende Turmaline aus Paraiba, Brasilien. *Z. Dt. Gemmol. Ges.* **1990**, *39*, 3–11.
5. Fritsch, E.; Shigley, J.E.; Rossman, G.R.; Mercer, M.E.; Muhlmeister, S.M.; Moon, M. Gem-quality cuprian-elbaite tourmalines from São José da Batalha, Paraíba, Brazil. *Gems Gemol.* **1990**, *26*, 189–205. [CrossRef]
6. Henn, U.; Bank, H.; Bank, F.H.; Platen, H.V.; Hofmeister, W. Transparent bright blue Cu-bearing tourmalines from Paraiba, Brazil. *Mineral. Mag.* **1990**, *54*, 553–557. [CrossRef]
7. Rossman, G.R.; Fritsch, E.; Shigley, J.E. Origin of color in cuprian elbaite from São José da Batalha, Paraíba, Brazil. *Am. Min.* **1991**, *76*, 1479–1484.
8. Milisenda, C.C. Cuprian tourmaline from Nigeria. *Z. Dt. Gemmol. Ges.* **2001**, *50*, 121–122.
9. Shigley, J.E.; Cook, B.C.; Laurs, B.M.; Bernardes de Oliveira, M. An update on "Paraíba" tourmaline from Brazil. *Gems Gemol.* **2001**, *37*, 260–276. [CrossRef]
10. Smith, C.P.; Bosshart, G.; Schwarz, D. Nigeria as a new source of copper-manganese-bearing tourmaline. *Gems Gemol.* **2001**, *37*, 239–240.
11. Laurs, B.M.; Simmons, W.; Falster, A. More on cuprian elbaite tourmaline from Nigeria. *Gems Gemol.* **2002**, *38*, 99–100.
12. Wentzell, C.Y. Copper-bearing color-change tourmaline from Mozambique. *Gems Gemol.* **2004**, *40*, 250–251.
13. Wentzell, C.Y.; Fritz, E.; Muhlmeister, S. More on copper-bearing color-change tourmaline from Mozambique. *Gems Gemol.* **2005**, *41*, 173–175. [CrossRef]
14. Milisenda, C.C. "Paraiba Turmaline" aus Quintos de Baixo, Rio Grande do Norte, Brasilien. *Z. Dt. Gemmol. Ges.* **2005**, *54*, 73–83.
15. Abduriyim, A.; Kitawaki, H. Cu- and Mn-bearing tourmaline—More production from Mozambique. *Gems Gemol.* **2005**, *41*, 360–361.
16. Abduriyim, A.; Kitawaki, H.; Furuya, M.; Schwarz, D. "Paraiba"-Type Copper-Bearing Tourmaline Form Brazil, Nigeria, and Mozambique: Chemical Fingerprint by LA-ICP-MS. *Gems Gemol.* **2006**, *42*, 4–21. [CrossRef]
17. Rondeau, B.; Delaunay, A. Les tourmalines cuprifères du Nigeria et du Mozambique. *Revue de Gemmologie AFG* **2007**, *160*, 8–13.
18. Furuya, M. Copper-bearing tourmalines from new deposits in Paraíba State, Brazil. *Gems Gemol.* **2007**, *43*, 236–239. [CrossRef]
19. Breeding, C.M.; Rockwell, K.; Laurs, B.M. New Cu-bearing tourmaline from Nigeria. *Gems Gemol.* **2007**, *43*, 384–385.
20. Laurs, B.M.; Zwaan, J.C.; Breeding, C.M.; Simmons, W.B.; Beaton, D.; Rijsdijk, K.F.; Befi, R.; Falster, A.U. Copper-Bearing (Paraiba-Type) Tourmaline from Mozambique. *Gems Gemol.* **2008**, *44*, 294–320. [CrossRef]
21. Karampelas, S.; Klemm, L. "Neon" Blue-to-Green Cu-and Mn-Bearing Liddicoatite Tourmaline. *Gems Gemol.* **2010**, *46*, 323–325.
22. Ertl, A.; Giester, G.; Schüssler, U.; Brätz, H.; Okrusch, M.; Tillmanns, E.; Bank, H. Cu- and Mn-Bearing Tourmalines from Brazil and Mozambique: Crystal Structures, Chemistry and Correlations. *Miner. Pet.* **2013**, *107*, 265–279. [CrossRef]
23. Okrusch, M.; Ertl, A.; Schüssler, U.; Tillmanns, E.; Brätz, H.; Bank, H. Major- and Trace-Element Composition of Paraíba-Type Tourmaline from Brazil, Mozambique and Nigeria. *J. Gemmol.* **2016**, *35*, 120–139. [CrossRef]
24. Katsurada, Y.; Sun, Z.; Breeding, C.M.; Dutrow, B.L. Geographic Origin Determination of Paraíba Tourmaline. *Gems Gemol.* **2019**, *55*, 648–659. [CrossRef]
25. Wang, H.A.O.; Krzemnicki, M.S.; Wälle, M.; Schultz-Guttler, R.A. Unsupervised Machine Learning for the Geographic Origin Determination of Cu-bearing Tourmaline. *J. Gemmol.* **2025**, *39*, 772–787. [CrossRef]
26. LMHC Standardised Gemmological Report Wording LMHC Information Sheet #6. Available online: https://www.lmhc-gemmology.org/wp-content/uploads/2023/06/LMHC-Information-Sheet_6_V8_2023.pdf (accessed on 7 August 2026).

27. Pasetti, L.; Borromeo, L.; Bersani, D.; Andò, S.; Schnellrath, J.; Hennebois, U.; Karampelas, S. Identification of Some Gem Quality Blue to Green Li-Tourmalines. *Minerals* **2024**, *14*, 44. [CrossRef]
28. Katsurada, Y.; Sun, Z. Cuprian Liddicoatite Tourmaline. *Gems Gemol.* **2017**, *53*, 34–41. [CrossRef]
29. Sun, Z.; Palke, A.C.; Breeding, C.M.; Dutrow, B.A. New Method for Determining Gem Tourmaline Species by LA-ICP-MS. *Gems Gemol.* **2019**, *55*, 2–17. [CrossRef]
30. Pezzotta, F.; Laurs, B.M. Tourmaline: The Kaleidoscopic Gemstone. *Elements* **2011**, *7*, 333–338. [CrossRef]
31. Merkel, P.B.; Breeding, C.M. Spectral Differentiation Between Copper and Iron Colorants in Gem Tourmalines. *Gem. Gemol.* **2009**, *45*, 112–119. [CrossRef]
32. Henry, D.J.; Novák, M.; Hawthorne, F.C.; Ertl, A.; Dutrow, B.L.; Uher, P.; Pezzotta, F. Nomenclature of the Tourmaline-Supergroup Minerals. *Am. Mineral.* **2011**, *96*, 895–913. [CrossRef]
33. Available online: https://www.gia.edu/gia-gem-project-tourmaline (accessed on 7 August 2026).
34. Krzemnicki, M.S.; Wang, H.A.O. Paraiba or Not? Cu-Bearing Tourmaline with a Distinct Fe Concentration. *J. Gemmol.* **2022**, *38*, 20–22. [CrossRef]
35. Taran, M.N.; Rossman, G.R.R. High temperature high pressure optical spectroscopy of ferric-iron bearing tourmaline. *Am. Mineral.* **2002**, *87*, 1148–1153. [CrossRef]
36. Brandstatter, F.; Niedermayr, G. Copper and Tenorite Inclusions in Cuprian-Elbaite Tourmaline from Paraiba, Brazil. *Gems Gemol.* **1994**, *30*, 178–183. [CrossRef]
37. Hartley, A. Native Copper Inclusions in a Cu-Bearing Tourmaline. *J. Gemmol.* **2018**, *36*, 203.
38. Wang, H.A.O.; Grolimund, D.; Franz, L.; Mathys, D.; Schultz-Güttler, R.; Krzemnicki, M.S. Further Characterisation of Native Copper Inclusions In-Bearing Tourmaline. *J. Gemmol.* **2023**, *38*, 427–429. [CrossRef]
39. Rossman, G.R. The geochemistry of gems and its relevance to gemology: Different traces, different prices. *Elements* **2009**, *5*, 159–162. [CrossRef]
40. Shabaga, B.M.; Fayak, M.; Hawthorne, F.C. Boron and lithium isotopic compositions as provenance indicators of Cu-bearing tourmalines. *Mineral. Mag.* **2010**, *74*, 241–255. [CrossRef]
41. Ludwig, T.; Marschall, H.R.; Pogge von Strandmann, P.A.E.; Shabaga, B.M.; Fayak, M.; Hawthorne, F.C. A secondary ion mass spectrometry (SIMS) re-evaluation of B and Li isotopic compositions of Cu-bearing elbaite from three global localities. *Mineral. Mag.* **2011**, *75*, 2485–2494. [CrossRef]
42. Gramaccioli, C.M. Application of mineralogical techniques to gemmology. *Eur. J. Mineral.* **1991**, *3*, 703–706. [CrossRef]
43. Fritsch, E.; Rondeau, B. Gemology: The developing science of gems. *Elements* **2009**, *5*, 147–152. [CrossRef]
44. Devouard, B.; Notari, F. Gemstones: From the naked eye to laboratory techniques. *Elements* **2009**, *5*, 163–168. [CrossRef]
45. Groat, L.A.; Giuliani, G.; Stone-Sundberg, J.; Sun, Z.; Renfro, N.D.; Palke, A.C. A Review of Analytical Methods Used in Geographic Origin Determination of Gemstones. *Gem. Gemol.* **2019**, *55*, 512–535. [CrossRef]
46. Available online: www.ssef.ch/new-source-of-paraiba-tourmalines-reportedly-discovered-in-ethiopia/ (accessed on 7 August 2026).
47. Available online: https://www.linkedin.com/feed/update/urn:li:activity:7476474837918613504/ (accessed on 7 August 2026).
48. Available online: https://blog.dgemg.com/en/research/222-cuprian-tourmalines-from-ethiopia.html (accessed on 7 August 2026).
49. Available online: https://www.linkedin.com/posts/vincent-pardieu-8697a32b_im-pleased-to-inform-you-that-the-field-share-7479230243820490753-9FpE/ (accessed on 7 August 2026).
50. Available online: https://www.rivistaitalianadigemmologia.com/en/2026/07/22/field-report-to-paraiba-tourmaline-rush-near-abuloo-ethiopia/ (accessed on 7 August 2026).
51. Available online: https://www.gia.edu/gia-news-press/gia-and-gubelin-gem-lab-confirm-new-source-of-copper-bearing-tourmaline-from-ethiopia (accessed on 27 August 2026).
52. Milisenda, C.C.; Guo, J. Neues Vorkommen kupferführender Turmaline in Äthiopien. *Z. Dt. Gemmol. Ges.* **2026**, *75*, 5–10.
53. Vertriest, W.; Palke, A.C.; Renfro, N.D. Field gemology: Building a Research Collection and Understanding the Development of Gem Deposits. *Gem. Gemol.* **2019**, *55*, 490–511. [CrossRef]
54. Yibas, B.; Reimold, W.U.; Armstrong, R.; Koeberl, C.; Anhaeusser, C.R.; Phillips, D. The Tectonostratigraphy, Granitoid Geochronology and Geological Evolution of the Precambrian of Southern Ethiopia. *J. Afr. Earth Sci.* **2002**, *34*, 57–84. [CrossRef]
55. Stern, R.J.; Ali, K.A.; Abdelsalam, M.G.; Wilde, S.A.; Zhou, Q. U–Pb Zircon Geochronology of the Eastern Part of the Southern Ethiopian Shield. *Precambrian Res.* **2012**, *206–207*, 159–167. [CrossRef]
56. Küster, D.; Romer, R.L.; Tolessa, D.; Zerihun, D.; Bheemalingeswara, K.; Melcher, F.; Oberthür, T. The Kenticha Rare-Element Pegmatite, Ethiopia: Internal Differentiation, U–Pb Age and Ta Mineralization. *Miner. Deposita* **2009**, *44*, 723–750. [CrossRef]
57. Billay, A.Y.; Kisters, A.F.M.; Meyer, F.M.; Schneider, J. The Geology of the Lega Dembi Gold Deposit, Southern Ethiopia: Implications for Pan-African Gold Exploration. *Mineral. Deposita* **1997**, *32*, 491–504. [CrossRef]

58. Tadesse, S. Genesis of the Shear Zone-Related Gold Vein Mineralization of the Lega Dembi Gold Deposit, Adola Gold Field, Southern Ethiopia. *Gondwana Res.* **2004**, *7*, 481–488. [CrossRef]
59. Giuliani, G.; Groat, L.A.; Marshall, D.; Fallick, A.E.; Branquet, Y. Emerald Deposits: A Review and Enhanced Classification. *Minerals* **2019**, *9*, 105. [CrossRef]
60. Tadesse, Y.; Tesfaye, M. *Geology of the Negele Area*; Memoir No. 11; Ethiopian Institute of Geological Surveys: Addis Ababa, Ethiopia, 1998; p. 124.
61. Gobena, H.; Belayneh, M.; Kebede, T.; Tesfaye, S.; Abraham, A. *Geology of the Dodola Area*; Memoir No. 10; Geological Survey of Ethiopia: Addis Ababa, Ethiopia, 1997; p. 144.
62. Gobena, H.; Belayneh, M.; Kebede, T.; Tesfaye, S. Dodola: Geological Map, Map Sheet NB-37-7 1998. Available online: https://shop.geospatial.com/product/2NRF7CRTSKKG4WJ8YN5ZXD2691/NB-37-7-DODOLA-Ethiopia-1-to-250000-Scale-Geological-Maps (accessed on 7 August 2026).
63. Kozyrev, V.; Girma, K.; Safonov, Y.; Bekele W/Michael; Gurbanovich, G.; Teweldemedhin, T.; Kaitukov, M.; Kuznetsov, J.; Tuliankin, U.; Arijapov, A. *Regional Geological and Exploration Work for Gold and Other Minerals in the Adola Goldfields*; Volume II: Regional geological mapping and prospecting; Ethiopian Mineral Resources Development Corporation: Addis Ababa, Ethiopia, 1985.
64. Worku, H.; Schandelmeier, H. Tectonic Evolution of the Neoproterozoic Adola Belt of Southern Ethiopia: Evidence for a Wilson Cycle Process and Implications for Oblique Plate Collision. *Precambrian Res.* **1996**, *77*, 179–210. [CrossRef]
65. Desta, B. *Preliminary Regional Geological Report on the Dodola (NB 37-7) 1:250,000 Scale Map-Sheet*; Geological Survey of Ethiopia: Addis Ababa, Ethiopia, 1978.
66. Teklay, M.; Kröner, A.; Mezger, K.; Oberhänsli, R. Geochemistry, Pb-Pb Single Zircon Ages and Nd-Sr Isotope Composition of Precambrian Rocks from Southern and Eastern Ethiopia: Implications for Crustal Evolution in East Africa. *J. Afr. Earth Sci.* **1998**, *26*, 207–227. [CrossRef]
67. Desta, B.; W/Michael, B. *Final Report on Mineral Exploration in Adola Area (Sidamo)*; Ethiopian Institute of Geological Surveys: Addis Ababa, Ethiopia, 1993; p. 202.
68. Watenphul, A.; Burgdorf, M.; Schlüter, J.; Horn, I.; Malcherek, T.; Mihailova, B. Exploring the Potential of Raman Spectroscopy for Crystallochemical Analyses of Complex Hydrous Silicates: II. Tourmalines. *Am. Mineral.* **2016**, *101*, 970–985. [CrossRef]
69. Jin, S.; Renfro, N.D.; Palke, A.C.; Ardon, A.; Homkrajae, A. Application of UV-Vis-NIR spectroscopy to gemmology. *Gem. Gemol.* **2019**, *55*, 456–473.
70. Taran, M.N.; Lebedev, A.S.; Platonov, A.N. Optical absorption spectroscopy of synthetic tourmalines. *Phys. Chem. Miner.* **1993**, *20*, 209–220. [CrossRef]
71. Mashkovtsev, R.I.; Smirnov, S.Z.; Shigley, J.E. The features of the Cu^{2+}-entry into the structure of tourmaline. *J. Struct. Chem.* **2006**, *47*, 252–257. [CrossRef]
72. Hennebois, U.; Delaunay, A.; Karampelas, S. Separating Elbaite from Liddicoatite Paraiba-Type Tourmaline. *J. Gemmol.* **2022**, *38*, 317–319. [CrossRef]
73. Milisenda, C.C.; Müller, S. REE Photoluminescence in Paraìba Type Tourmaline from Mozambique. In Proceedings of the 35th International Gemmological Conference, Windhoek, Namibia, 11–15 October 2017; pp. 71–73.
74. Lenz, C.; Nasdala, L.; Talla, D.; Hauzenberger, C.; Seitz, R.; Kolitsch, U. Laser-Induced REE^{3+} Photoluminescence of Selected Accessory Minerals—An "Advantageous Artefact" in Raman Spectroscopy. *Chem. Geol.* **2015**, *415*, 1–16. [CrossRef]
75. Vereshchagin, O.S.; Rozhdestvenskaya, I.V.; Frank-Kamenetskaya, O.V.; Zolotarev, A.A.; Mashkovtsev, R.I. Crystal chemistry of Cu-bearing tourmalines. *Am. Mineral.* **2013**, *98*, 1610–1616. [CrossRef]
76. Vereshchagin, O.S.; Setkova, T.V.; Rozhdestvenskaya, I.V.; Frank-Kamenetskaya, O.V.; Deyneko, D.V.; Pokholok, K.V. Synthesis and crystal structure of Ga-rich, Fe-bearing tourmaline. *Eur. J. Mineral.* **2016**, *28*, 593–599. [CrossRef]
77. Vereshchagin, O.S.; Wunder, B.; Britvin, S.N.; Frank-Kamenetskaya, O.V.; Wilke, F.D.H.; Zolotarev, A.A.; Vlasenko, N.S.; Shilovskikh, V.V. Synthesis and crystal structure of Pb-dominant tourmaline. *Am. Mineral.* **2020**, *105*, 1589–1592. [CrossRef]
78. Ertl, A.; Bačík, P. Considerations About Bi and Pb in the Crystal Structure of Cu-Bearing Tourmaline. *Minerals* **2020**, *10*, 706. [CrossRef]

Disclaimer/Publisher's Note: The statements, opinions and data contained in all publications are solely those of the individual author(s) and contributor(s) and not of MDPI and/or the editor(s). MDPI and/or the editor(s) disclaim responsibility for any injury to people or property resulting from any ideas, methods, instructions or products referred to in the content.